NIPPON STEEL TECHNICAL REPORT No. 61 APRIL 1994

UDC669.14.018.8:669.18

Advances in Stainless Steelmaking Technology

Ryoji Tsujino*1
Ryuji Nakao*1
Katsuhiko Kato*2
Ryoichi Hisatomi*2
Shin-ya Kitamura*1
Hironori Takano*3
Hiroaki Morishige*3
Hiroshi Hirata*1

Abstract:

A high-speed and high-efficiency decarburization technology was established for the manufacture of austenitic stainless steel at Hikari Works. This technology improves the efficiency of decarburization efficiency and shortens the refining time by the AOD combined blowing whereby the effect of the hot spot formed by hard-blown top oxygen is fully utilized. At Yawata Works, on the other hand, decarburization technology was established for the manufacture of ferritic stainless steel. It achieves optimum load distribution between LD converter with high carbon turndown and VOD with high-speed decarburization by vacuum control to prevent bumping and by intense stirring with increased ladle bottom injection argon. A new decarburization index S-BOC indicating the oxidation of carbon in preference to chromium is proposed to explain the effect of combined blowing. The world's first technology of manufacturing metal catalyst carrier through continuous casting was established by developing an optimum mold powder and an appropriate technique for high-precision addition of REM into the mold.

1. Introduction

In a nearly one century since the birth of stainless steels around 1910[1], stainless steelmaking technology has made outstanding progress, and various new processes have been employed in combination in the commercial production of stainless steels[2]. This article reviews the history of technology development for the manufacture of austenitic and ferritic stainless steels. Of the recent stainless steelmaking technologies, combined blowing with argon oxygen decarburization (AOD), dephosphorization of high-chromium hot metal, high-efficiency and high-purity steel production with vacuum oxygen decarburization (VOD), and metal catalyst carrier production are described.

Table 1 shows the changes in austenitic and ferritic stainless steelmaking technologies at Nippon Steel.

2. Austenitic Stainless Steelmaking Technology

Nippon Steel produces austenitic stainless steels represented by SUS 304 at its Hikari Works. The stainless steelmaking process comprises 60tons/heat electric arc furnace (EAF), AOD, and continuous caster (CC) steps. In the EAF step, stainless steel scrap and ferroalloys, such as ferrosilicon and ferronickel, are preheated by kerosene burners and melted by alternating-current (AC) arc in a new melting furnace (NMF)[3] of the one-power supply, two-

*1 Technology Development Bureau
*2 Yawata Works
*3 Hikari Works

Table 1 Changes in stainless steelmaking technologies at Nippon Steel

Year	Austenitic stainless steels	Ferritic stainless steels	
	Hikari Works	Yawata Works	Muroran Works
1951		Stainless steelmaking test started with 30-t EAF	
⋮			
1960	10-t EAF started up (operated until 1979)		
1961	40-t EAF started up (operated until 1986)		
1963		Stainless steelmaking test started with 2-t test furnace	
1965			Stainless steelmaking started with 50-t test furnace
1966	60-t DH started up (operated until 1974) Vertical slab caster started up (single-strand)		
1967		30-t EF-DH started 75-t LD-DH-IC test started	
1968	60-t EAF started up (operated until 1986)	75-t LD-DH process brought into semi-commercial operation	RH started (iron ore decarburization process established)
1969	Vertical bloom caster started up (single-strand)		Use of dephosphorized hot metal started
1970			Work started on development of RH-OB process
		Yawata Iron & Steel and Fuji Iron & Steel merged into Nippon Steel	
		USSR-type (vertical) caster started up	
1971		50-t LD-VOD process put to commercial operation	Bow-type caster started up
1972			RH-OB operation started with double-pipe nozzle
1974	60-t AOD started up (EAF-AOD-CC process)		Vacuum control technology established for RH-OB process
1975			RH-OB-FD process established
1977			Converter capacity increased from 50 to 120 t/heat in line with steelmaking plant rationalization
1978	Ladle alloy addition unit installed		
1979		150-t VOD installed	
1980		Production started by combined-blown LD-OB process Production started by single-slag LD process with hot metal ladle soda ash injection (SIDP) method	
1981	Vertical bloom caster converted to two-strand design AOD coolant transport and addition unit started up		
1982	AOD Ar/O_2 ratio optimization process (AOD-O process) established	Converter direct receipt method	Single-slag LD converter steelmaking started with process to remove silicon and phosphorus by blowing oxygen into hot metal ladle
1983			Technology established for carburization refining with combined-blown converter
1984		Chrome ore smelting reduction process started on test basis	
1985	60-t new melting furnace of one-power supply, two-furnace type started up		Converter capacity increased from 120 to 280 t/heat in line with steelmaking plant rationalization
1986	AOD air top blowing unit started up		
1988		Stainless steelmaking by torpedo car hot metal pretreatment	
1989	2/10-t combination VIM furnace started up	Efficiency improved by VOD lance water cooling and functional division	Final tap made (cumulative production of 1,538,000 tons)
1990	Horizontal caster started up (two-strand)		
1991	AOD top oxygen blowing unit started up	Optimum distribution of decarburization load between converter and VOD (VOD oxygen flow rate increase)	
1992	AOD high-speed blowing unit started up		

furnace type. After decarburization and slag reduction (desulfurization) in the AOD furnace, the steel is tapped into a ladle. In the ladle, the melt is stirred by argon bubbling for temperature and chemistry homogenization before being totally fed into the continuous caster. There are three continuous caters: a vertical slab caster, a vertical bloom caster, and a horizontal bloom caster[4].

Regarding the AOD refining technology, various development and commercialization results have been achieved to date with the aim of raising productivity and improving product quality. Among them are optimization of the oxygen-argon blowing pattern according to specific carbon content requirement (AOD-O process)[5], reduction in sulfur and oxygen contents to ultralow levels through aluminum addition and slag composition control[6], and improvement in refractories quality. A 2/10-ton combination vacuum induction melting (VIM) furnace was installed for small-lot production of high-alloy steel with high purity, utilizing flux refining[7].

2.1 AOD combined blowing technology

AOD combined blowing (top and bottom blowing) is being introduced to increase the total oxygen flow rate and thermal feasibility by adding top blowing[8,9]. The conventional top blowing process performed soft blowing with a bath surface depression ratio L/L_0 of 0.05 or less (where L is the bath surface depression depth caused by top blowing and L_0 is the static bath depth). This soft blowing was designed to promote post combustion, increase the heating rate of the molten steel, and suppress the oxidation of chromium[9,10]. The decarburization rate is thus considered to be lower than in bottom blowing at the same oxygen flow rate. Work was started on the development of efficient combined blowing technology. Preliminary experiments were conducted with a 100-kg furnace and a 6-ton combined-blown converter. The experimental results obtained were applied to the actual process to improve the decarburization rate and efficiency at the same oxygen flow rate as in bottom blowing.

2.1.1 Analysis of top-blown hot spot reaction by 100-kg furnace experiment

Fig. 1 shows the effects of top blowing, bottom blowing, and combined blowing on the relationship between the carbon concentration and the decarburization rate at the same oxygen flow rate of 100 Nl/min in the 100-kg furnace. Top blowing was kept on the hard blow side at $L/L_0 = 0.1$ to promote the reaction of top-blown oxygen with the steel bath. For combined blowing, the ratio of top-blown to bottom-blown oxygen was set at 1:1. The solid marks in **Fig. 1** indicate the region where chromium is oxidized and the slag is increased in Cr_2O_3 content and solidified. Judgment of slag solidification was made from video images during the blowing.

The decarburization rate improves from top blowing, bottom blowing to combined blowing in that order. The same order holds for the decrease of the carbon concentration at which the decarburization rate drops and slag solidifies. Video images showed

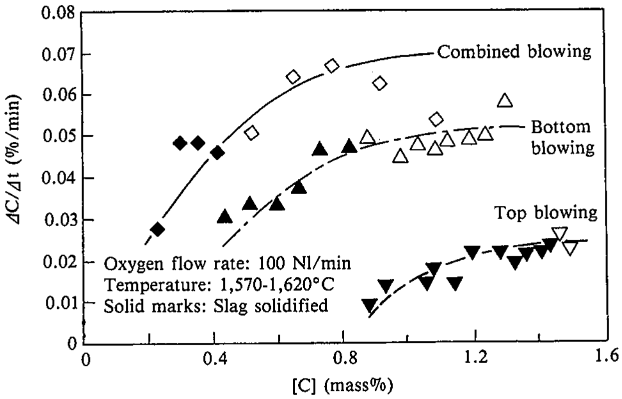

Fig. 1 Effect of blowing method on relationship between carbon concentration and decarburization rate (100-kg furnace)

that the bath surface was covered with slag solidified by the formation of Cr_2O_3, which prevented the top-blown oxygen from reaching the molten steel thereby to retard the oxygen-steel reaction. Analysis of hot spot spectra by two-color radiation thermometry confirmed that the top-blown hot spot temperature was a high 2,350°C on the average for both top blowing and combined blowing. The molten steel in the bath surface near the top-blown hot spot was sampled using a copper lump (50 mm in diameter). The sample was sectioned and examined by an optical microscope and electron-probe microanalyzer (EPMA). Chromium oxides were identified on the sample cross section. This result confirmed that the hot spot has a high temperature and forms a high-oxygen region (chromium oxide layer), and that the oxygen concentration (chromium oxide layer) is reduced more drastically in combined blowing than in top blowing. It was thus found that combined blowing promotes the Cr_2O_3 reduction reaction at the high-temperature hot spot and that intense bottom-blown gas stirring accelerates the decarburization of the melt by promoting the transfer of oxygen from the hot spot.

$$(Cr_2O_3)+3\underline{C}=2\underline{Cr}+3CO(g) \quad \cdots\cdots(1)$$

2.1.2 Determination of optimum top blown-to-bottom blown oxygen ratio by 6-ton converter test; proposal of new refining index

Fig. 2 shows the effect of the top-blown oxygen ratio (= top-blown oxygen/total blown oxygen) on the average decarburization rate at and above the carbon concentration of 0.5 mass% in the 6-ton combined-blown converter test. Each top blowing

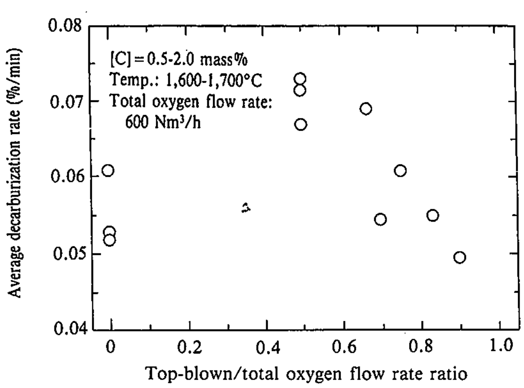

Fig. 2 Effect of top-blown/total oxygen flow rate ratio on average decarburization rate

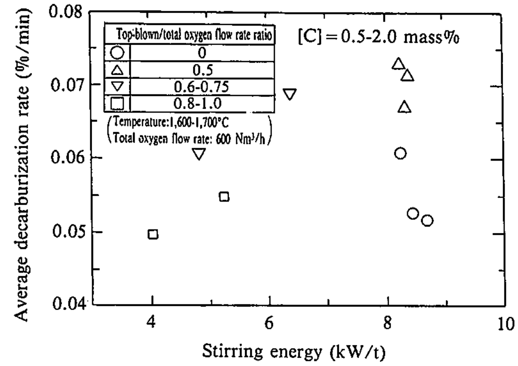

Fig. 3 Effect of stirring energy on average decarburization rate

run was hard blowing with $L/L_0 = 0.1$. As the 100-kg furnace test did, the 6-ton furnace test confirmed that combined blowing can improve the decarburization rate compared with bottom blowing, and verified the existence of an optimum top-blown oxygen ratio for the decarburization rate.

Fig. 3 shows the effect of the molten steel stirring energy $\dot{\varepsilon}$ on the average decarburization rate. The stirring energy $\dot{\varepsilon}$ was calculated from the equation of Kai et al.[11] taking into consideration the stirring force of top-blown oxygen as well. The stirring energy $\dot{\varepsilon}$ being equal, combined blowing marks a higher decarburization rate than top blowing. Under combined blowing, the decarburization rate comes to a saturation point when the stirring energy $\dot{\varepsilon}$ exceeds 6 kW/t, as is separately confirmed by the results of the 100-kg furnace test. This points to the importance of promoting decarburization by Cr_2O_3 at the top-blown hot spot when stirring is intense at 6 kW/t or over.

According to the above test results, a preferential decarburization index that indicates the oxidation of carbon in preference to chromium was studied. BOC[12], ISCO[13], and CROI[14] have been applied to stainless steel for its similitude to plain carbon steel. These indices do not take into account the temperature of the heat that has a large impact on the decarburization of stainless steel and the top blown hot spot reaction that is essential for combined blowing. It was found that they could not uniformly express the decarburization performance of bottom blowing, top blowing and combined blowing as exhibited in the results of the 100-kg and 6-ton furnace tests.

The decarburization of stainless steel depends on the balance between the oxidation and reduction of chromium. Assuming that the transfer of carbon to the reaction interface depends on the mixing time (τ) and interfacial carbon concentration ([%C]*), the reduction of chromium is expressed by $(1/t)\cdot([\%C]-[\%C]^*)$. Assuming that the oxidation of chromium depends on the oxygen flow rate and slag volume per unit weight of molten steel, it is expressed by $(Q_{O_2}/W)\cdot W_s$. As a new preferential decarburization index for stainless steel, S-BOC is defined as given by

$$\text{S-BOC}=\frac{Q_{O_2}}{(W/\tau)\cdot[\%C]}\cdot\frac{W_s}{(1-[\%C]^*/[\%C])} \quad \cdots\cdots(2)$$

where Q_{O_2} is total oxygen flow rate (Nm³/min); W is weight of molten steel (t); W_s is weight of slag per unit weight of molten steel (kg/t). Equation (2) can be finally reduced to Eq. (3) by assuming the following conditions: 1) the carbon and chromium concentrations are constant; 2) the mixing time τ is expressed as $\tau \propto W^{2/9}\dot{\varepsilon}^{-1/3}$ under intense stirring; 3) the reaction rate is controlled by mass transfer; 4) combined blowing is the sum of top blowing and bottom blowing; and 5) the CO partial pressure P_{CO} is expressed as $2Q_{O_2}/(2Q_{O_2} + Q_d)$.

$$\text{S-BOC} = \frac{[\%\,Cr]}{[\%\,C]} \cdot \frac{W_S}{W^{7/9}} \cdot \frac{2Q_{O_2}}{2Q_{O_2}+Q_d} \cdot \frac{1}{\dot{\varepsilon}'^{1/3}}\left(\frac{Q_{O_2-B}}{C_1K_1} + \frac{Q_{O_2-T}}{C_2K_2}\right) \quad \cdots\cdots(3)$$

where $\dot{\varepsilon}'$ is stirring energy density (kW/m^3); Q_d is inert gas flow rate (Nm^3/min); K_1 is $10^{-13800/T_1+8.76}$ [where T_1 is steel bath temperature (K)]; K_2 is $10^{-13800/T_2+8.76}$ [where T_2 is hot spot temperature (K)]; C_1, C_2 are coefficients related to top blowing conditions; subscript B is bottom blowing; and subscript T is top blowing. Equation (3) consists of: 1) [C] and [Cr] concentration terms; 2) slag and steel weight terms; 3) P_{CO} term; 4) stirring energy term; and 5) temperature term. Each of C_1 and C_2 is a function of both the temperature and area of the top-blown hot spot. They were determined from the results of the 6-ton furnace test.

Fig. 4 shows the 100-kg and 6-ton furnace test data and actual operation data as arranged by the S-BOC index. The S-BOC index can uniformly express both bottom blowing and combined blowing. Decarburization at the high-temperature top-blown hot spot should improve the decarburization efficiency under combined blowing. This index also suggests that the decarburization of the heat can be accelerated further by raising the top-blown hot spot temperature while holding the stirring energy at a certain level.

2.1.3 Establishment of high-speed and high-efficiency AOD combined blowing technology

Results of the 100-kg and 6-ton furnace tests indicate that decarburization by combined blowing can be effectively promoted by utilizing the high-temperature top-blown hot spot reaction with intense stirring at 6 kW/t or over. This finding was applied to actual AOD furnaces. First, optimum top and bottom blowing ratios were determined for the same total oxygen flow rate of 4,000 Nm^3/h as used for bottom blowing. A water-cooled laval nozzle lance was adopted for hard top blowing. **Fig. 5** shows the relationship between h/d_0[15], an index of post combustion control in top-blown converters and dC/dO_2, the amount of decarburization per oxygen flow rate at a carbon concentration of 0.5 mass % or above. The bottom-blown oxygen stirring energy $\dot{\varepsilon}$ exceeds 6 kW/t in each case, and d/d_0 is given by

$$h/d_0 = H/d_0 - H_c/d_0 \quad \cdots\cdots(4)$$

$$H_c/d_0 = 4.12P - 1.86 \quad \cdots\cdots(5)$$

$$Q_{O_2-T} = 0.968nA(P+1.033)\times 10^4 \quad \cdots\cdots(6)$$

where H is lance gap (mm); H_c is potential core length (mm); h is free jet length (mm); d_0 is nozzle throat diameter (mm); P is nozzle front pressure (kg/cm^2); n is nozzle hole number; and A is nozzle throat area (m^2). As evident from **Fig. 5**, h/d_0 and dC/dO_2 are almost linearly related to each other, and dC/dO_2 increases with decreasing h/d_0. dC/dO_2 for combined blowing exceeds that for bottom blowing when h/d_0 is less than 60 or in the hard-blowing region.

It was confirmed that the temperature rise per unit amount of decarburization is lower in combined blowing with h/d_0 being less than 60 or in the hard-blowing region than in bottom blowing. The conventional AOD combined blowing process[9,10] promotes post combustion, raises the heating rate, and retards the oxidation of chromium. The oxygen flow rate being equal, the decarburization rate is lower than achievable with only bottom blowing. The high-speed and high-efficiency AOD combined blowing process described here performs hard top blowing. The hard top blowing practice increases the amount of oxygen reacting with the steel bath by utilizing the high-temperature reaction at the top-blown hot spot, which is advantageous for decarburization, and provides a decarburization rate higher than obtainable with bottom blowing alone at the same oxygen flow rate. The new AOD combined blowing process succeeded in shortening the refining time by about 3 min and reducing the silicon reductant consumption by 1.7 kg/t.

In December 1992, the AOD waste gas cooling equipment was modified to permit total oxygen flow rates up to 9,000 Nm^3/h. A high-speed combined blowing test was conducted by applying the above-mentioned combined blowing results to the AOD furnace. In the test, combined blowing was applied to the carbon concentration region of 0.05 wt% or above, the bottom-blown oxygen flow rate was kept constant at 4,000 Nm^3/h, and the top-blown oxygen flow rate was varied. The lance gap was held constant at 2 m.

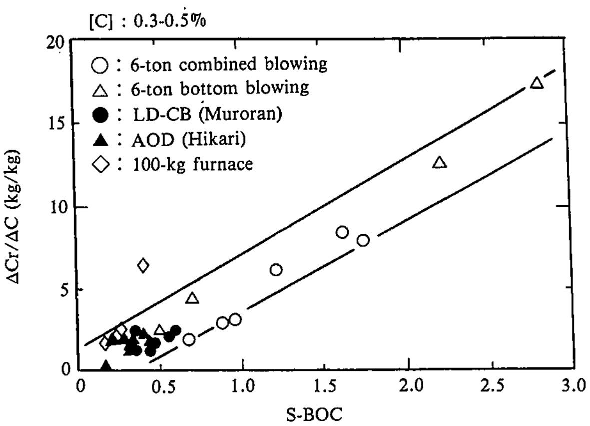

Fig. 4 Relationship between S-BOC and ΔCr/ΔC

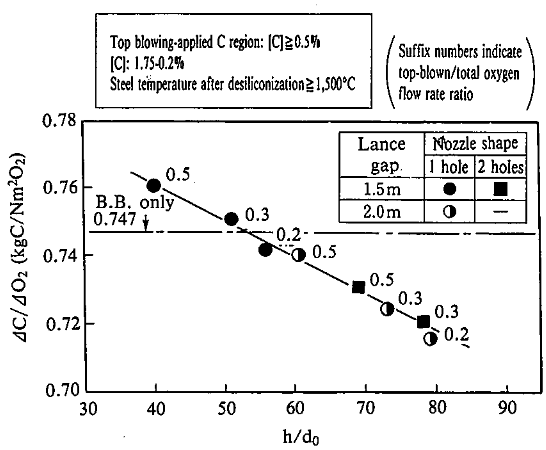

Fig. 5 Relationship between h/d_0 and $\Delta C/\Delta O_2$

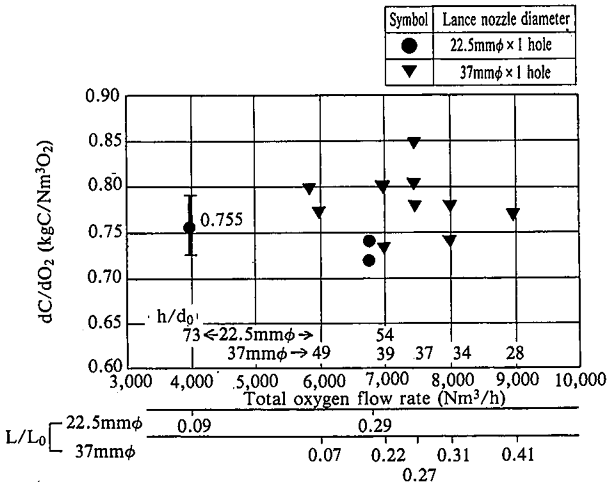

Fig. 6 Relationship between total AOD oxygen flow rate and dC/dO_2 ($[C] \geqq 0.5\%$)

In **Fig. 6**, the test results are shown in terms of the total oxygen flow rate versus dC/dO_2. The values of h/d_0 and L/L_0 are also given. With the lance gap kept constant in the test, increasing the total oxygen flow rate decreased h/d_0, increased L/L_0, and produced hard blowing. Although the data vary in some degree, dC/dO_2 remained practically constant despite an increase in the total oxygen flow rate, resulting in increased decarburization rate and much shorter refining time. An AOD refining time of 40 min or less, including the reduction treatment, was accomplished for some grades of stainless steel.

An AOD combined blowing technology with unprecedentedly high blowing speed and efficiency was established by intensifying oxygen top blowing and enhancing the reaction of top-blown oxygen with the steel bath. It utilizes high-temperature reactions at the top-blown hot spot while maintaining the stirring intensity at a sufficiently high level.

3. Ferritic Stainless Steelmaking Technology

3.1 High-chromium hot metal dephosphorizing technology

Dephosphorization of high-chromium hot metal is strongly influenced by the carbon content of hot metal. When hot metal with a nearly saturated carbon content is used, it can be dephosphorized with a low-cost burnt lime flux. Accordingly, using a lime (CaO)-fluorspar (CaF_2)-iron oxide flux, basic experiment was conducted in a small furnace. It was found as a result that hot metal dephosphorization can be efficiently performed under suppressed oxidation of chromium, by increasing the oxygen weight ratio of lime to iron oxide (CaO/O) and decreasing the oxidizing power and increasing the basicity of the flux. Upon this finding, 250-ton torpedo car test was conducted at the hot metal pretreatment station of Yawata Works. The test method is as shown in **Fig. 7**. The test was made without making any equipment modification. A flux composed of about 60% CaO, 22% CaF_2 and 18% iron oxide was injected through an injection lance at the rate of about 50 kg/t, and oxygen for temperature compensation was blown through a top lance at about 4 Nm^3/t.

Fig. 8 shows the effect of the CaO/O ratio of injection flux (where the amount of top-blown oxygen is not included in O) on the dephosphorization volumetric rate constant and the drop

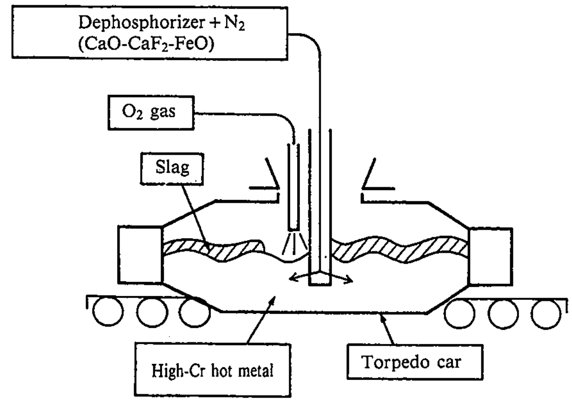

Fig. 7 Schematic illustration of 250-ton test apparatus

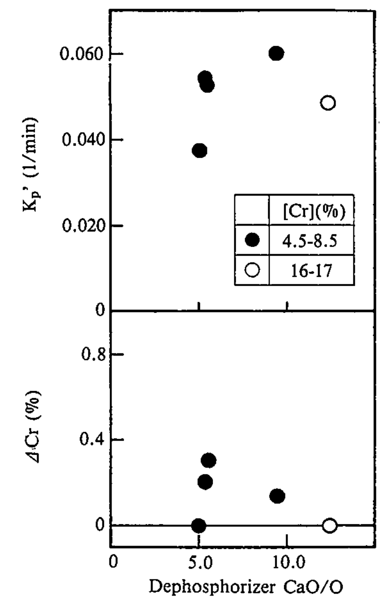

Fig. 8 Effect of flux CaO/O ratio on dephosphorization volumetric rate constant and chromium content drop after dephosphorization

of chromium content after dephosphorization. As the basic experiments did, this test show that increasing the CaO/O ratio promotes dephosphorization and suppresses the oxidation of chromium. The temperature drop was about 50K. The top-blown oxygen flow rate had little effect on dephosphorization and chromium oxidation. This is probably because the dephosphorization and decarburization reaction sites were separated in such a way that the dephosphorization reaction proceeded at the interface of the flux rising through the bath and that the decarburization reaction proceeded at the top-blown hot spot. The above results indicate that high-chromium hot metal can be efficiently dephosphorized with a limited temperature drop and chromium oxidation by optimizing the injection flux composition and utilizing top-blown oxygen.

3.2 High-efficiency and high-purity VOD steelmaking technology

Yawata Works produces ferritic stainless steel by a combination of LD-VAC and LD-OB process. Described below are the high-speed, high-efficiency VOD oxygen blowing and high-purity stainless steel manufacturing technology developed at Yawata

Works.

3.2.1 High-efficiency stainless steelmaking technology by VOD high-speed oxygen blowing

Yawata's ferritic stainless steelmaking process consists of preliminary decarburization, chromium addition in the LD-OB furnace, finish decarburization in the VOD furnace, and continuous casting by a vertical casting machine. D.C. Hilty et al.[16] and J. Chipman[17] report that in stainless steel refining, the carbon content depends on the chromium content and temperature of the melt and the partial pressure of CO. As indicated by S-BOC, turndown at a high carbon content is effective in retarding chromium oxidation in the converter. The high carbon turndown means a low turndown temperature. The high carbon turndown, however, increases the VOD load and prolongs the treatment time, resulting in lower productivity in VOD. The VOD oxygen flow rate was increased to avoid a productivity drop and to optimize the distribution of the decarburization load between the converter and the VOD unit.

Fig. 9 shows the relationship between the carbon content and the decarburization oxygen efficiency in the LD-OB furnace. The decarburization oxygen efficiency decreases as the carbon content falls past the 0.7-0.8% level. Turndown around this carbon region is effective, and the wear of the converter refractory lining is reduced by lowering the turndown temperature following the Arrhenius equation[18]. Equipment modification and operating practice adopted to suit high-speed decarburization from a high-carbon region in the VOD furnace are described next. In terms of equipment, ejector and condenser reinforcement was made to cope with a drastic increase in the generation of waste gas. In terms of operation, measures were taken against violent spitting and overflow due to a rapid CO reaction in the bath. Namely, the shield bottom depression depth and the bottom gap were optimized to reduce the amount of metal spattering out of the system. The problem of metal overflow was solved by clarifying the overflow mechanism and controlling overflow according to the standard free energy change ΔG involving the reduction of chromium oxide by carbon. The relationship between ΔG and the overflow is shown in **Fig. 10**.

3.2.2 VOD high-purity steelmaking technology

The technology of reducing the carbon content of ferritic stainless steel to an ultralow level is described here. Stirring conditions are a predominant factor in the VOD decarburization treatment[19] and are closely related to the implementation of

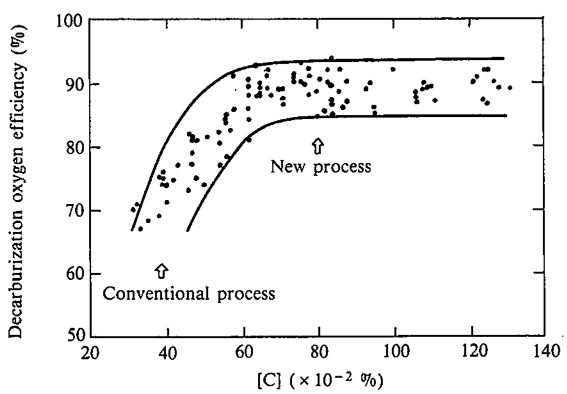

Fig. 9 Change in decarburization oxygen efficiency in converter

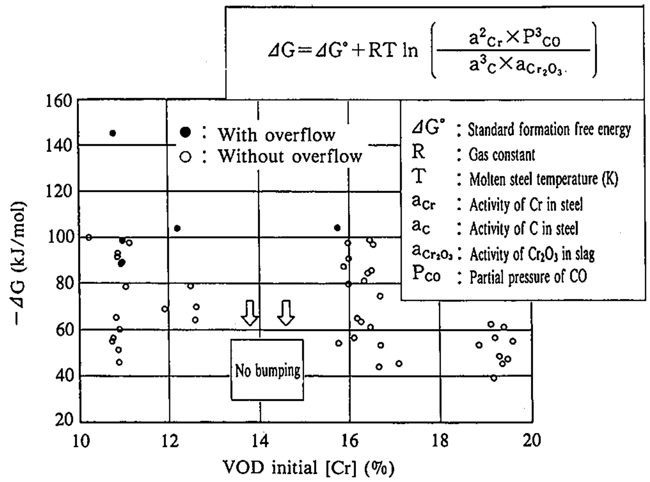

Fig. 10 Relationship between ΔG and initial chromium content

high-efficiency decarburization treatment. Plant test levels are shown in **Table 2**. The test results are given in **Fig. 11**, where K_1 and K_2 are overall reaction rate constants for decarburization periods I and II, respectively. The carbon content is 0.14 to 0.02% in the decarburization period I and is 0.02% or less in the decarburization period II. The decarburization rate increased with increasing stirring power, except for the test levels 3 to 5 with multiple porous plugs. The decarburization reaction rate controlling step was evaluated by assuming that it can be evaluated in the same way as done by the RH reaction model of Sumida et al.[20] The recirculation rate was calculated by the equation of Sano[21] that was multiplied by coefficients to suit plant data.

As shown in **Fig. 12**, the VOD operation during the decarbu-

Table 2 Plant test levels

Test level No. (Graph symbol)	1 (○)	2 (△)	3 (●)	4 (■)	5 (▲)
Central PP flow rate (Nl/min)	300	800	150	300	400
Eccentric PP flow rate (Nl/min)	—	—	150	300	400
Bottom-blown gas flow rate (Nl/min·t)	2.2	7.3	2.5	5.0	7.3
Top-blown gas flow rate (Nl/min·t)	247	303	278	278	303

PP: Porous plug

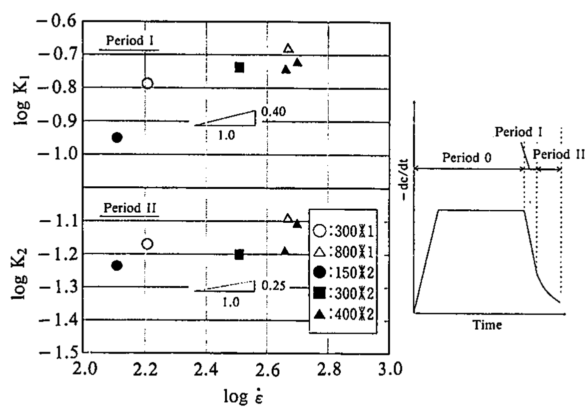

Fig. 11 Effect of stirring energy on overall reaction rate constant during carburization period

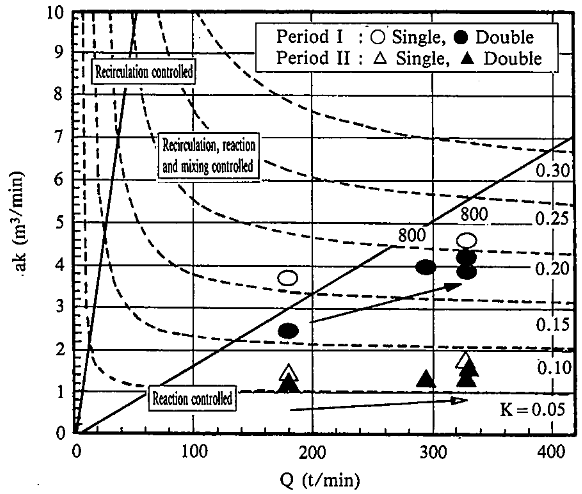

Fig. 12 Relationship between recirculation rate Q and capacity coefficient ak

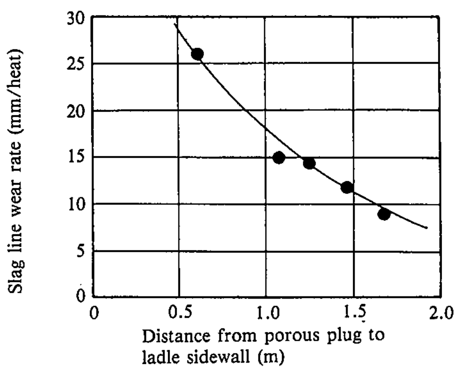

Fig.13 Wear of ladle refractory lining

rization periods I and II fell in the reaction rate controlling region. Increasing stirring energy probably increased the effective interfacial area a, the mass transfer coefficient k at the reaction site, and the decarburization rate. The decrease in the decarburization rate with increase in the number of porous plugs may be explained by the decrease in the plume eye area or the effective interfacial area a. The decarburization rate was retarded during the period II, probably because the melt is difficult to decarburize internally in this region.

Fig. 13 shows the wear of the ladle refractory lining according to the position of bottom-blown gas injection. It was found as a result that the use of multiple porous plugs increases the refining cost by increasing the wear of ladle refractory lining, and that intense stirring through a single porous plug at the center of the ladle is optimal.

4. Manufacturing Technology of Metal catalyst carrier

Nippon Steel had worked on the development of stainless steel as metal support for automotive catalytic converters since 1986. As such a material, ferritic heat-resistant steel of 20% chromium-5% aluminum composition was difficult to produce by the continuous casting process. The steel is now continuously cast, rolled into foil, and fabricated into a honeycomb with a complicated thermal fatigue-resistant joint structure.

This metal catalyst carrier material is composed basically of 20% chromium, 5% aluminum, and rare-earth metals (REM).

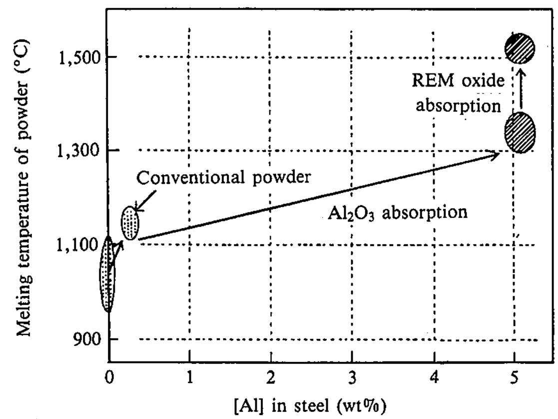

Fig. 14 Change in melting temperature of mold powder with aluminum content of molten steel

Titanium is added to improve toughness as hot-rolled strip, and the REM content is set at 0.08% so that the highest possible oxidation resistance can be secured.

4.1 Problems with slab production

In the early stages of commercial application, the mold powder so widely varied in properties that cast slabs often had longitudinal surface cracks and cast-in slag entrapment. The slab surfaces had to be ground to the depth of more than 10 mm to get rid of such surface defects. Further, REM elements added in wire form into the molten steel in the mold occasionally enriched and segregated in the slab subsurface, and reduced the slab's hot workability causing cracks during hot rolling.

The following were essential issues for the manufacture of metal support foil steel by the continuous casting process:

(1) Development of mold powder useful to improve the slab surface quality

(2) Development of a technique to feed REM wire into mold steel with high precision and uniformity

4.2 Development of mold powder

When high-aluminum steel is continuously cast, the aluminum of the molten steel generally reacts with the SiO_2 of the mold powder to increase the Al_2O_3 content and basicity (CaO/SiO_2 ratio) of the molten powder. The resultant increase in viscosity and melting temperature drastically lowers the lubricity an essential property of the molten powder. Since this steel contains REM as well as 5% aluminum, the viscosity and melting temperature of the mold powder are raised further. **Fig. 14** shows the effects of aluminum and REM on the melting temperature of the mold powder. To prevent these changes in the mold powder property as far as possible, Li_2O, NaF and TiO_2 were added, and the Al_2O_3 and SiO_2 contents were reduced. To prevent the crystallization of Al_2O_3-MgO spinel, the MgO content was held under 5%.

4.3 Development of technique for uniformly adding REM wire into mold

When added into the ladle or tundish, REM not only are low in yield but also lead to nozzle clogging with REM oxides. They are therefore added directly into the mold in wire form. The optimum REM wire melting position was studied by fluid dynamical calculation, and the relationship between the REM wire melting position and the segregation of REM in cast slabs was evaluated. **Fig. 15** shows the segregation of REM in slabs in the

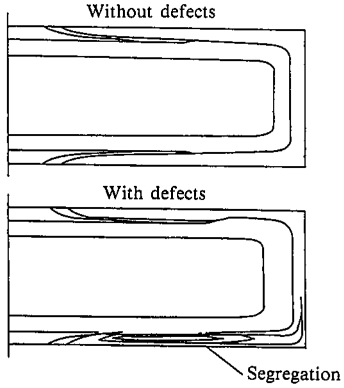

Fig. 15 Results of calculation of REM distribution in slabs

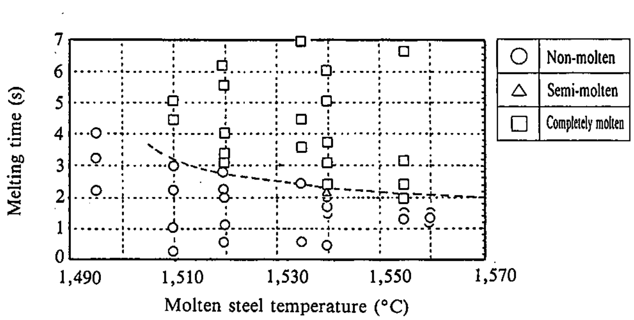

Fig. 16 Effect of molten steel temperature on wire melting

thickness direction as obtained by fluid dynamical calculation. The REM segregation can be prevented by melting the REM wire near the bottom end of the main discharge stream from the immersion nozzle. To melt it stably in the target position in the mold, factors governing the REM wire melting mechanism and time were investigated. **Fig. 16** shows the effect of molten steel temperature on the melting time of the REM wire immersed in the molten steel in laboratory test. Values of melting time theoretically estimated by Eqs. (7) and (8) are also shown. They agree well with the measured values. Melting time by wire type and operating condition can thus be estimated by theoretical calculation.

$$t_m = \frac{\rho C_p r}{2h} \ln\{(T_e - T_0)/(T_e - T_m)\} \quad \cdots\cdots(7)$$

$$\frac{1}{h} = \frac{r_{REM}}{\lambda_{REM}} + \frac{t}{\lambda_{Fe}} + \frac{1}{h_0} \quad \cdots\cdots(8)$$

where ρ is density of molten steel (kg/m^3); C_p is specific heat of molten steel (kcal/kgK); r is radius of wire after immersion (initial wire + buildup) (m); λ is thermal conductivity (kcal/m•sK); h is overall heat transfer coefficient ($kcal/m^2 \cdot sK$); h_0 is heat transfer coefficient of wire ($kcal/m^2 \cdot sK$); t is covering thickness of wire (m); r_{REM} is radius of REM core in the wire (m); T_e is temperature of molten steel (K); T_0 is initial temperature of wire (K); and T_m is liquidus temperature of wire covering (K).

Optimum wire adding conditions in accord with casting conditions were found, and the positive segregation of REM was successfully prevented, making it possible to continuously cast the metal catalyst carrier substrate steel for the first time in the world.

5. Conclusions

The development history of stainless steelmaking technologies has been reviewed, and, in particular, the latest progress therein has been described.

(1) For austenitic stainless steels, Hikari Works recorded high decarburization oxygen efficiency and short refining time by the AOD combined blowing technology that utilizes the effect of the top-blown hot spot by hard blowing, and established high-speed, high-efficiency decarburization technology.
(2) For ferritic stainless steels, Yawata Works established the technology of realizing optimum load distribution between high-carbon converter turndown and high-speed VOD finish decarburization by vacuum control for prevention of VOD bumping and by intense stirring with increased ladle bottom-blown argon flow rate.
(3) S-BOC was proposed as a new decarburization refining index that can explain the effectiveness of the combined blowing technology and indicate the oxidation of carbon in preference to chromium.
(4) The technology whereby metal catalyst carrier can be continuously cast was established for the first time in the world through the development of an optimum mold powder and technique of adding REM wire into the mold with high precision.

References

1) History of Stainless Steelmaking Technology. Nippon Metal Industry, 1983, p.6
2) Ejima, A.: 44th and 45th Nishiyama Memorial Lecture, 1977, p.3
3) Makino, N. et al.: Seitetsu Kenkyu. (335), 13 (1989)
4) Kubota, M. et al.: CAMP-ISIJ. 4, 214 (1991)
5) Ikehara, Y. et al.: Proc. Electric Furnace Conf. 43, 183 (1985)
6) Ikehara, Y. et al.: Tetsu-to-Hagané. 70, A37 (1984)
7) Yanagi, Y. et al.: CAMP-ISIJ. 3, 1241 (1990)
8) Yamada, K. et al.: Tetsu-to-Hagané. 68, S973 (1982)
9) Ushiyama, H. et al.: Electric Furnace Steelmaking. 52, 20 (1981)
10) Heinke, R. et al.: Proc. Int. Oxy. Steelmak. Cong. 1987, p.313
11) Kai, T. et al.: Tetsu-to-Hagané. 68, 1946 (1982)
12) Kitamura, S. et al.: Tetsu-to-Hagané. 72, 47 (1986)
13) Nakanishi, K. et al.: Tetsu-to-Hagané. 64, S169 (1978)
14) Kishimoto, Y. et al.: Tetsu-to-Hagané. 76, 1924 (1990)
15) Hirai, M. et al.: Tetsu-to-Hagané. 73, 1117 (1987)
16) Hilty, D.C. et al.: J.I.S.I. 180, 116 (1955)
17) Chipman, J.: J.I.S.I. 180, 97 (1977)
18) Soumiya, S. et al.: 48th and 49th Nishiyama Memorial Lecture, 1977, p.190
19) Iwaoka, S.: Tetsu-to-Hagané. 63 (2), A1 (1977)
20) Sumida, N. et al.: Kawasaki Steel Technical Report. 152 (1983)
21) Sano, M. et al.: Tetsu-to-Hagané. 68, 2451 (1982)